IEEE Open Journal of
Circuits and Systems

Received 4 December 2022; revised 7 February 2023; accepted 12 March 2023. Date of publication 27 March 2023; date of current version 6 April 2023.

Digital Object Identifier 10.1109/OJCAS.2023.3262204

Polychronous Oscillatory Cellular Neural Networks for Solving Graph Coloring Problems

RICHELLE L. SMITH (Graduate Student Member, IEEE), AND THOMAS H. LEE (Fellow, IEEE)

Department of Electrical Engineering, Stanford University, Stanford, CA 94305, USA
This article was recommended by Associate Editor D. Linaro.

CORRESPONDING AUTHOR: R. L. SMITH (e-mail: smithrl@stanford.edu)

This work was supported in part by the Sang Samuel Wang Stanford Graduate Fellowship and in part by the ARCS Foundation Northern California Fellowship (William K. Bowes, Jr. Foundation Scholar).

ABSTRACT This paper presents polychronous oscillatory cellular neural networks, designed for solving graph coloring problems. We propose to apply the Potts model to the four-coloring problem, using a network of locally connected oscillators under superharmonic injection locking. Based on our mapping of the Potts model to injection-locked oscillators, we utilize oscillators under divide-by-4 injection locking. Four possible states per oscillator are encoded in a polychronous fashion, where the steady state oscillator phases are analogous to the time-locked neuronal firing patterns of polychronous neurons. We apply impulse sensitivity function (ISF) theory to model and optimize the high-order injection locking of the oscillators. CMOS circuit design of a polychronous oscillatory neural network is presented, and coloring of a geographic map is demonstrated, with simulation results and design guidelines. There is good agreement between theory and Spectre simulation.

INDEX TERMS CMOS, cellular neural network (CNN), computing, graph coloring, impulse sensitivity function (ISF), neuromorphic computing, polychronization.

I. INTRODUCTION

BRAIN-INSPIRED systems are promising alternatives to traditional von Neumann computing [1], [2], [3], [4]. One compelling approach is cellular neural networks, which are a neuromorphic architecture inspired by biological retinas [5], [6]. A cellular neural network (CNN) is composed of an array of cells in which each cell is connected to its neighbors. The CNN performs computations in the continuous time domain, utilizing the physical dynamics of the circuit.

Various approaches to implement the cells of a CNN have been studied. Early approaches realized the cells with operational amplifiers or operational transconductance amplifiers [5], which require large area and power. Recently, the use of memristors for the CNN cells has been explored [7], [8], [9], [10], but memristors are not yet widely available in commercial CMOS processes. To address these challenges, we propose to use time-domain signaling with CNNs, instead of traditional amplitude-domain signaling. Advantages of the time-domain approach include compatibility with CMOS scaling and operation with lower supply voltage [11].

To encode information in the timing or phase of waveforms, we can draw inspiration from the polychronous spiking neurons in the brain [12], [13], which fire spikes at different moments in time to encode information in the sequence of neuronal firing. We propose to implement each cell of the CNN as a CMOS oscillator under high-order injection locking, with local connections to neighboring oscillators. The result is a polychronous oscillatory cellular neural network. The integrated CMOS oscillator approach provides the benefits of a small form factor and compatibility with standard CMOS foundries, leveraging existing infrastructure for design and manufacturing.

In this paper, we present CMOS oscillatory CNNs with polychronization, and illustrate how they can be used to solve graph coloring problems, by mapping the Potts model to high-order injection-locked oscillators with local connections. In Section II, we briefly review the fundamentals of graph coloring problems and Potts model theory. In

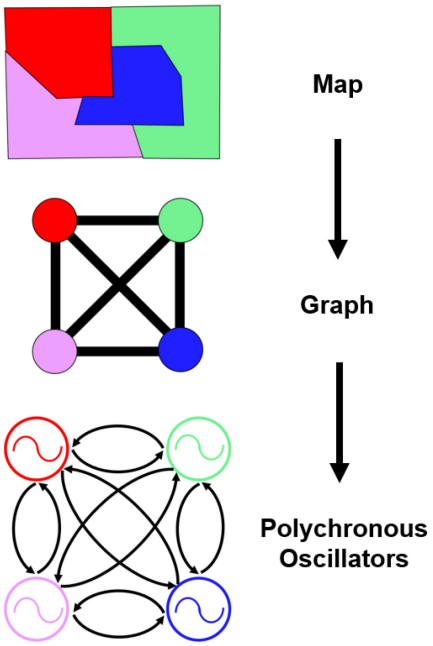

FIGURE 1. Mapping of four-color graph coloring problem to polychronous oscillatory cellular neural network.

Section III, we demonstrate how to form an oscillatory CNN with superharmonic injection locking, by using the Potts model. We apply impulse sensitivity function (ISF) theory to model the injection locking of the oscillator network. In Section IV, we present a CMOS circuit design of a polychronous oscillatory CNN and a coloring example of a geographic map, with simulation results.

II. FUNDAMENTALS OF GRAPH COLORING AND POTTS MODEL

A. GRAPH COLORING

Graph coloring is a nondeterministic polynomial-time hard (NP-hard) computation problem with a variety of applications, including scheduling tasks, ride-sharing, register allocation, mobile radio frequency assignment, and puzzles such as Sudoku [14]. Graph coloring is a combinatorial optimization problem, where each vertex of a graph is assigned a color (label). The goal is to compute the minimum number of colors such that no two vertices sharing a common edge connection are assigned the same color [14], shown in Fig. 1. It has been shown that any map lying in a plane can be converted to a planar graph and four colors suffice to ensure that no neighboring vertices share the same color. More generally, the Four Color Theorem states that no more than four colors are needed to color any planar graph [15].

The use of oscillators to solve graph coloring problems has previously been studied. Reference [16] focuses on analysis and numerical simulation only and does not present a hardware design. Reference [17] presents an approach to solving graph coloring problems using vanadium dioxide oscillators, while [9] presents a memristor-based approach. However, a more general approach with a circuit hardware mapping, that is compatible with established CMOS foundry technology, is needed.

B. POLYCHRONOUS OSCILLATORY CNN FOR GRAPH COLORING

We propose a polychronous oscillatory CNN architecture, based on the Potts model, that solves the planar graph coloring problem, while only requiring one oscillator per vertex of the graph. Four possible states per oscillator are encoded in a polychronous fashion, where the steady state oscillator phases are analogous to the time-locked neuronal firing patterns of polychronous neurons. The allowable oscillator phases are separated by 90°, and each phase corresponds to a different color.

C. POTTS MODEL THEORY

We now briefly review the Potts model, which was originally developed to study phase transitions in ferromagnetic materials. Each lattice point in the material has a spin value. The individual spins interact with neighboring spins and dynamically adjust their spin states. The Potts model allows for N possible spin states [18]. The planar Potts model is defined for a network of interacting spins confined to a plane. Each spin points to one of q equally spaced angles [18]

$$\theta_n = \frac{2\pi n}{q} \qquad n = 0, 1, \ldots, q-1 \tag{1}$$

The nearest neighbor interaction depends only on the relative angles between the spins. The neighboring spins interact and change their spin states until the total system energy reaches the minimum.

The total energy of the system, or Potts Hamiltonian, is defined as [18]

$$H = -\sum_{i,j} J_{i,j} J\left(\theta_i - \theta_j\right) - \sum_i h_i, \tag{2}$$

where $J(\theta)$ is periodic in 2π and h_i is the external field located at each spin. In the planar Potts model,

$$J\left(\theta_i - \theta_j\right) = \cos\left(\theta_i - \theta_j\right). \tag{3}$$

Then, the Hamiltonian becomes

$$H = -\sum_{i,j} J_{i,j} \cos\left(\theta_i - \theta_j\right) - \sum_i h_i, \tag{4}$$

where the summation is performed over interacting spins and $J_{i,j}$ represents the interactions between spins. $J_{i,j}$ can be positive (ferromagnetic) or negative (antiferromagnetic). From the second law of thermodynamics, the system's spins arrange themselves to minimize the free energy (Hamiltonian). In the next section, we show how to use high-order injection-locked oscillators to map the Potts model to the graph coloring problem.

III. IMPLEMENTING AN OSCILLATORY CNN WITH POTTS MODEL

A. MAPPING THE POTTS MODEL TO OSCILLATORY CNN

We propose to map the Potts model to the planar graph coloring problem, where the graph vertices can take the four values $\{0°, 90°, 180°, 270°\}$. The weights of the edges are represented by $J_{i,j}$, the connection between vertices. Such a graph can be mapped to planar graph coloring problems, where each vertex's spin (phase) represents the color. The total number of available spin states is therefore 4^N, where N is the number of spins (oscillators) in the system. For negative connections ($J_{i,j} < 0$), the Potts Hamiltonian is minimized when adjacent (interacting) spins are not the same state, for the maximum possible number of interacting spins. This condition is analogous to the requirement that adjacent vertices differ in color in the graph coloring problem.

Replacing vertices with oscillators and the graph edges with connections between the oscillators realizes a polychronous oscillatory CNN, for properly discretized oscillator phases. This discretization can be realized through superharmonic injection locking. All oscillators are injected with a master pump signal at $N \cdot f_0$, where f_0 is the natural oscillation frequency of the oscillators and N is an integer. The steady state phase of the oscillators corresponds to a global Lyapunov function of the same form as the Hamiltonian of the Potts model, as will be shown in Section III-D.

To model the injection-locked oscillatory neural network, we begin by reviewing the concept of the ISF [19], [20], [21]. We then derive the steady-state equations of the oscillatory CNN.

B. ISF AND INJECTION LOCKING THEORY

ISF theory treats an oscillator as a linear, periodically time-varying (LPTV) system. The response of a free-running oscillator to an injected current impulse, $i(t) = \delta(t - \tau)$, is a phase step that persists indefinitely. The impulse response can be written [19]

$$h_\phi(t, \tau) = \frac{\Gamma(\omega_0 \tau)}{q_{\max}} u(t - \tau), \tag{5}$$

where $u(t)$ is the unit step function, $q_{\max}$ is the maximum charge swing across the terminals of the injected current impulse, and ω_0 is the free-running oscillation frequency. $\Gamma(\omega_0\tau)$ is the ISF and is dimensionless and periodic, with period 2π. The ISF captures the sensitivity of an oscillator to an injected impulse at phase $\omega_0\tau$. An oscillator is linear time-variant in the sense that the induced phase change from an input current impulse depends on τ, the time instant at which the impulse is applied.

The superposition integral captures the response of the oscillator's phase, $\phi(t)$, to an arbitrary injection current, $i_{\text{inj}}(\tau)$,

$$\phi(t) = \int_{-\infty}^{\infty} h_\phi(t, \tau)\, i_{\text{inj}}(\tau) d\tau. \tag{6}$$

In the following analysis, it is easier to work with the non-normalized ISF [20], [22]

$$\tilde{\Gamma}(x) = \frac{\Gamma(x)}{q_{\max}}, \tag{7}$$

which has units of [1/coulomb]. $\Gamma(x)$ is generally an intrinsic property of the specific oscillator topology, while $\tilde{\Gamma}(x)$ depends on $q_{\max}$ and, therefore, the capacitance at the injection node.

We can substitute (5) and (7) into (6) to obtain

$$\phi(t) = \int_{-\infty}^{t} \tilde{\Gamma}(\omega_0 \tau)\, i_{\text{inj}}(\tau) d\tau. \tag{8}$$

Next, we differentiate with respect to time, [20]

$$\frac{d\phi}{dt} = \tilde{\Gamma}(\omega_0 t)\, i_{\text{inj}}(t). \tag{9}$$

We now consider an oscillator with free-running frequency, ω_0, under injection from a signal of frequency ω_{inj}, that is near ω_0. The preceding analysis has been carried out in the free-running oscillator's frame of reference. We can transform the frame of reference to the injection current's frame of [20]. θ is the phase between the periodic injection current, $i_{\text{inj}}(t)$, and the oscillation voltage waveform and satisfies

$$\theta = \phi_{\text{osc}} - \phi_{\text{inj}}. \tag{10}$$

ϕ_{osc} is the phase of the oscillator voltage's fundamental tone, while ϕ_{inj} is the phase of the injection current's fundamental tone [23]. Thus, we can rewrite (9) in terms of θ,

$$\frac{d\theta}{dt} = \omega_0 - \omega_{\text{inj}} + \tilde{\Gamma}\left(\omega_{\text{inj}} t + \theta\right) i_{\text{inj}}(t). \tag{11}$$

In the steady state, (11) can be rewritten in time-averaged form as the pulling equation [20]

$$\frac{d\theta}{dt} = \omega_0 - \omega_{\text{inj}} + \frac{1}{T_{\text{inj}}} \int_{T_{\text{inj}}} \tilde{\Gamma}\left(\omega_{\text{inj}} t + \theta\right) \cdot i_{\text{inj}}(t) dt, \tag{12}$$

where T_{inj} is the period of the injection current over which time-averaging takes place.

Since both the ISF and injection current are periodic, they can be expressed as Fourier series. This allows the averaging integral in (12) to be rewritten as [22], [23]

$$\frac{d\theta}{dt} = \omega_0 - \omega_{\text{inj}} + \frac{1}{2}\left[\frac{I_{\text{inj},0}\tilde{\Gamma}_0}{2} + \sum_{n=1}^{\infty} |I_{\text{inj,n}}\tilde{\Gamma}_{\text{n}}| \cos\left(n\theta + \angle\tilde{\Gamma}_{\text{n}} - \angle I_{\text{inj,n}}\right)\right]. \tag{13}$$

The Fourier coefficient representation results in compact expressions for the locking region, as will be shown.

Under the lock condition, $\frac{d\theta}{dt} = 0$. Then, from (12), the lock characteristic, $\Omega(\theta)$, is given by [20]

$$\Omega(\theta) = \omega_{\text{inj}} - \omega_0 = \frac{1}{T_{\text{inj}}} \int_{T_{\text{inj}}} \tilde{\Gamma}\left(\omega_{\text{inj}} t + \theta\right) \cdot i_{\text{inj}}(t) dt. \tag{14}$$

It can be seen that under lock, the periodic injection current contributes a constant phase shift over each injection period.

We now consider the case of superharmonic injection, where the injected frequency is in the vicinity of a multiple of the free-running frequency Under lock, the relationship between ω_{inj} and the oscillation frequency, ω_{osc}, satisfies

$$M\omega_{\text{inj}} = N\omega_{\text{osc}}, \tag{15}$$

where M and N are coprime, positive integers. θ now satisfies

$$\theta = \phi_{\text{osc}} - \frac{M}{N}\phi_{\text{inj}}. \tag{16}$$

Then, from (12), the generalized pulling equation is [23]

$$\frac{d\theta}{dt} = \omega_0 - \frac{M}{N}\omega_{\text{inj}} + \frac{1}{NT_{\text{inj}}}\int_{NT_{\text{inj}}} \tilde{\Gamma}\left(\frac{M}{N}\omega_{\text{inj}}t + \theta\right)\cdot i_{\text{inj}}(t)dt. \tag{17}$$

Consider the case of a sinusoidal injection current at the Nth superharmonic (implying $M = 1$),

$$i_{\text{inj}}(t) = I_{\text{inj}}\cos(N\omega_{\text{osc}}t), \tag{18}$$

where I_{inj} is the amplitude of the injection current.

Then, the lock characteristic (14) simplifies to

$$\Omega(\theta) = \frac{1}{2}|I_{\text{inj}}\tilde{\Gamma}_{\text{N}}|\cos\left(N\theta + \angle\tilde{\Gamma}_N\right), \tag{19}$$

which can alternatively be derived from (13). Taking the extremes of (19), the N^{th} harmonic lock region is bounded by

$$\begin{aligned}\omega_{\text{low}} &= N\omega_{\text{osc}} - \frac{1}{2}NI_{\text{inj}}|\tilde{\Gamma}_{\text{N}}|\\ \omega_{\text{high}} &= N\omega_{\text{osc}} + \frac{1}{2}NI_{\text{inj}}|\tilde{\Gamma}_{\text{N}}|\,,\end{aligned} \tag{20}$$

where ω_{low} and ω_{high} are the lower and upper lock range limit, respectively [22]. To increase the lock range, either $|\tilde{\Gamma}_{\text{N}}|$ or I_{inj} can be increased.

C. USING DIVIDE-BY-4 INJECTION LOCKING TO SOLVE PLANAR GRAPH COLORING

We now derive the steady state solution for the oscillatory CNN. Each oscillator in the neural network is under simultaneous injection at several frequencies from the master pump signal and the connections to other oscillators. Each oscillator is under injection from one pump signal at frequency ω_{pump}. For the i^{th} oscillator, superposition can be applied to the current injection from the connections to k other oscillators at frequency ω_{osc}. From (17), the pulling equation for a single oscillator is

$$\begin{aligned}\frac{d\theta_i}{dt} = \omega_0 &- \frac{M}{N}\omega_{\text{pump}}\\ &+ \frac{1}{NT_{\text{pump}}}\int_{NT_{\text{pump}}}\tilde{\Gamma}\left(\frac{M}{N}\omega_{\text{pump}}t + \theta_i\right)\cdot i_{\text{pump}}(t)dt\\ &+ \sum_{j=1}^{k}\frac{1}{T_{\text{osc, j}}}\int_{T_{\text{osc, j}}}\tilde{\Gamma}\left(\omega_{\text{osc, j}}t + \theta_i\right)\cdot i_{\text{osc, j}}(t)dt.\end{aligned} \tag{21}$$

The first two addends in the first line capture the frequency mismatch between the free-running frequency and pump frequency, the addend in the second line captures the injection of the pump current, and the addend in the third line captures the injection from the connected oscillators. This equation determines the steady-state phase of each oscillator in the network and the system of these equations captures the solution to the graph coloring problem. In our example with four possible states per oscillator and the pump signal at $4f_0$, $M = 1$ and $N = 4$. Under locking to the pump, the pump frequency is four times the oscillator frequency, and we refer to this as divide-by-4 injection locking. For the interactions between connected oscillators, the injection frequency is close to the natural free-running frequency, so $M = 1$ and $N = 1$.

ISF theory also provides a theoretical basis for why divide-by-4 injection locking results in four stable oscillation modes (quadrature output phases separated by 90°). Under lock, θ_0 is stable if and only if the lock characteristic has a negative slope at θ_0. That is, the condition for a stable mode is [20]

$$\Omega'(\theta_0) = \frac{\partial\Delta\omega}{\partial\theta}\bigg|_{\theta=\theta_0} < 0. \tag{22}$$

The lock characteristic is periodic in θ with a period of $\frac{2\pi}{N}$. Since θ_0 may take any value from 0 to 2π, the lock characteristic, $\omega(\theta)$, completes four sinusoidal cycles over the possible values of θ. Thus, $\omega(\theta)$ has four regions of equally spaced negative slopes, resulting in four stable oscillation modes that correspond to quadrature phases.

D. DERIVATION OF GLOBAL MINIMUM SOLUTION

In this section, we establish the mapping between the objective function describing the graph coloring problem and the Lyapunov function describing the hardware. We demonstrate the ground state of a Lyapunov function describing the polychronous oscillatory cellular neural network is equivalent to the global minimum of an objective function describing the graph coloring problem.

The i^{th} oscillator that is connected to k other oscillators can also be described in a compact form using Kuramoto's equation [24]

$$\frac{d\theta_i}{dt} = \sum_{j=1}^{k}K_{i,j}\sin\left(\theta_i - \theta_j\right) + K_p\sin(N\theta_i). \tag{23}$$

$K_{i,j}$ captures the interaction between oscillators, as well as the ISF. K_p captures the pump current as well as the ISF. We assume that all oscillators oscillate at the same frequency.

The global Lyapunov function for (23) exists [25], [26] and can be written as

$$\begin{aligned}E(t) = \frac{N}{2}&\sum_{i,j,i\neq j}K_{i,j}\cos\left(\theta_i - \theta_j\right)\\ &+ \sum_i K_p\cos(N\theta_i).\end{aligned} \tag{24}$$

Next, we confirm that the polychronous oscillatory cellular neural network seeks to minimize the global Lyapunov function over time. We can confirm this by showing $\frac{dE(t)}{dt} \leq 0$.

Taking the derivative of (24) and applying the chain rule, we obtain

$$\frac{dE(t)}{dt} = \sum_{i=1} \frac{\partial E(t)}{\partial \theta_i} \cdot \frac{d\theta_i}{dt}. \tag{25}$$

Next, we evaluate $\frac{\partial E(t)}{\partial \theta_i}$.

$$\begin{aligned}\frac{\partial E(t)}{\partial \theta_i} &= \frac{N}{2} \sum_{j=1, i\neq j} K_{i,j} \frac{\partial}{\partial \theta_i} \cos\left(\theta_i - \theta_j\right) \\ &\quad + \frac{N}{2} \sum_{j=1, i\neq j} K_{j,i} \frac{\partial}{\partial \theta_i} \cos\left(\theta_j - \theta_i\right) + K_p \frac{\partial}{\partial \theta_i} \cos(N\theta_i) \\ &= -\frac{N}{2} \sum_{j=1, i\neq j} K_{i,j} \sin\left(\theta_i - \theta_j\right) \\ &\quad + \frac{N}{2} \sum_{j=1, i\neq j} K_{j,i} \sin\left(\theta_j - \theta_i\right) - K_p N \sin(N\theta_i) \\ &= -N \sum_{j=1, i\neq j} K_{i,j} \sin\left(\theta_i - \theta_j\right) - N K_p \sin(N\theta_i) \\ &= -N \frac{d\theta_i}{dt} \end{aligned} \tag{26}$$

The last line of (26) was obtained by substituting (23).

Substituting (26) into (25), we obtain

$$\frac{dE(t)}{dt} = -N \sum_{i=1} \left(\frac{d\theta_i}{dt}\right)^2 \leq 0. \tag{27}$$

Therefore, we have shown (24) is a global Lyapunov function that is minimized over time by the oscillatory neural network.

We now show that the global Lyapunov function (24) is of the same form as the Potts Hamiltonian (2). For divide-by-four injection locking with $N = 4$ and the quadrature output phases $\theta_i = \{0°, 90°, 180°, 270°\}$, $\cos(N\theta_i)$ evaluates to 1, 0, -1, and 0, which are constants. The global Lyapunov function then simplifies to

$$E(t) = -\sum_{i,j,i\neq j} A_{i,j} \cos\left(\theta_i - \theta_j\right) - A, \tag{28}$$

where $A_{i,j}$ is a scaled term capturing the interaction between oscillators. A is a constant representing the pump that is analogous to the external field term in (4). We observe the form of the global Lyapunov function (28) is equivalent to the Potts Hamiltonian (4).

IV. CIRCUIT DESIGN AND SIMULATION RESULTS

A. OSCILLATORY CNN CIRCUIT DESIGN

This section presents illustrative circuit design and simulation results for a high-order, injection-locked oscillatory CNN machine designed in 65nm CMOS. The first graph to be colored is shown in Fig. 1, and the four regions of the map correspond to the four oscillators (vertices of the graph). The six edges on the graph correspond to the twelve connections between oscillators (each edge is bidirectional), shown in Fig. 2. Each vertex of the graph (oscillator) is connected to the adjacent vertices, thus requiring four colors for a valid coloring.

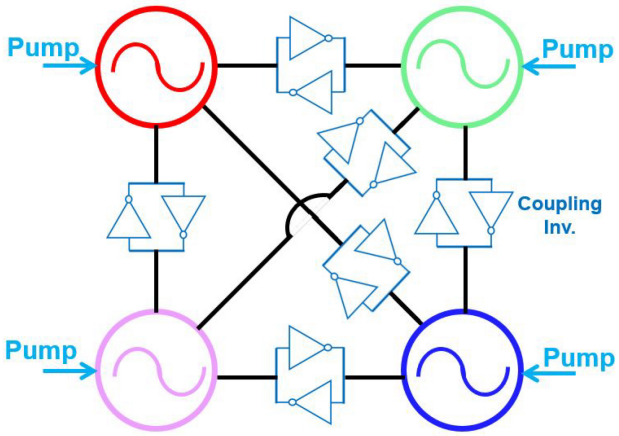

FIGURE 2. Schematic of the polychronous oscillatory CNN, with local connection elements shown between the four oscillators. The oscillation frequency is f_0, while the pump frequency is $4f_0$, resulting in quadrature oscillator output phases.

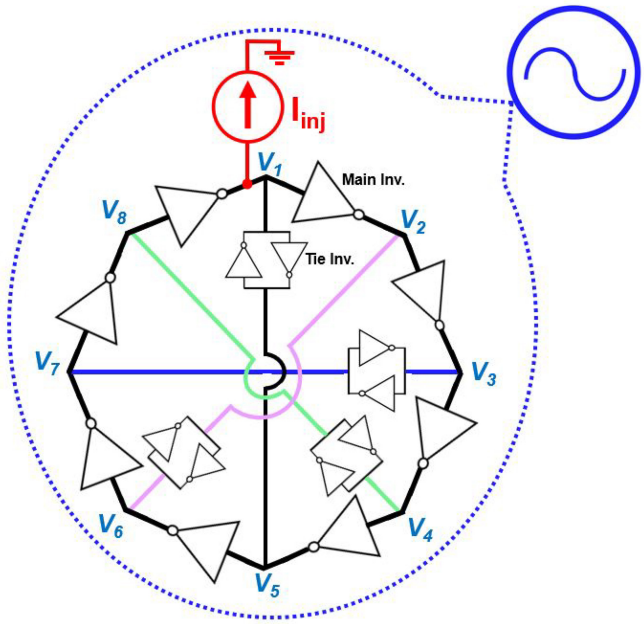

FIGURE 3. Schematic of an octahedral oscillator serving as the unit oscillator cell.

The basic cell of the polychronous oscillatory neural network is an oscillator under simultaneous injection from a pump signal ($4f_0$ in this case) and other oscillators (f_0). For the oscillator cell, the ring oscillator is chosen over an LC-oscillator, due to its more compact area, wider locking range, and faster lock time.

The connection between oscillators and pump injections can be realized by inverters acting as tunable transconductors. The connections between oscillators are implemented with CMOS inverters. Each connection is a bidirectional inverting connection, injected at each oscillator's V_1 node (see Fig. 3). In practice, adjusting the relative strength of the connecting inverters can be implemented with tunable

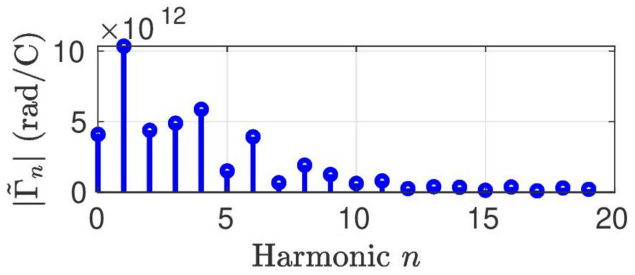

FIGURE 4. Impulse sensitivity function of octahedral oscillator. Asymmetric rise and fall times of the output waveform enhance the harmonics of $|\tilde{\Gamma}_n|$.

g_m cells. For example, additional parallel unit inverters can be enabled or disabled. A pump signal is injected to all oscillators at the V_1 node and each oscillator is subject to the same injection current excitation from the master pump source. In the simulation, sinusoidal current sources are used to implement the pump injection currents. In practice, the pump injection can be implemented as a sinusoidal voltage superimposed on the gate bias voltage to generate current injection through inverters. This entirely inverter-based design is digital-CMOS friendly and amenable to porting across technology nodes.

The schematic of the high-order, injection-locked oscillatory neural network is shown in Fig. 2, while the unit oscillator schematic is shown in Fig. 3. The inverters in the oscillator are intentionally sized for asymmetric rise and fall times of the oscillator voltage waveform [23], with $W_n = 4W_p$. This choice increases $|\tilde{\Gamma}_4|$ and enables easier locking to the pump signal, as will be shown. This is because asymmetric rise and fall times enable the fourth-harmonic current injection to produce positive and negative phase shifts of unequal magnitude on the rising and falling edges. As a result, a larger net phase shift accumulates over an oscillation period and this fixed phase shift per period enables the frequency shift necessary to lock the oscillator to an injection. Thus, asymmetric rise and fall times enhance the harmonic content of the ISF, compared to the case of an oscillator waveform with symmetric rise and fall times.

The device sizings are shown in Table 1. The design involves inverters of three different sizings: the oscillator main inverters, oscillator tie inverters, and coupling inverters between oscillators. The oscillator inverters are shown in Fig. 3. The larger inverters (such as the inverter between V_1 and V_2 nodes) are referred to as the main inverters. The smaller inverters connecting opposite nodes (such as the inverter between V_1 and V_5 nodes) are referred to as tie inverters. The main inverters are sized to be 3 times larger than the tie inverters, to satisfy the oscillator startup condition. The inverters coupling the neighboring oscillators are referred to as the coupling inverters. C_L is the load capacitance added between each node of the oscillator and ground. The oscillator's free running frequency is close to 250 MHz, while the pump signal is a 1 GHz sinusoid with 10 μA amplitude.

TABLE 1. Polychronous oscillatory CNN design parameter values.

Component	Parameter Value
$W_{\text{p, osc, main}}$	0.25 μm × 3
$W_{\text{n, osc, main}}$	1 μm × 3
$W_{\text{p, osc, tie}}$	0.25 μm
$W_{\text{n, osc, tie}}$	1 μm
L_{osc}	270 nm
$W_{\text{p, coupling}}$	0.5 μm
$W_{\text{n, coupling}}$	0.25 μm
L_{coupling}	60 nm
C_{L}	4 fF
V_{DD}	0.5 V

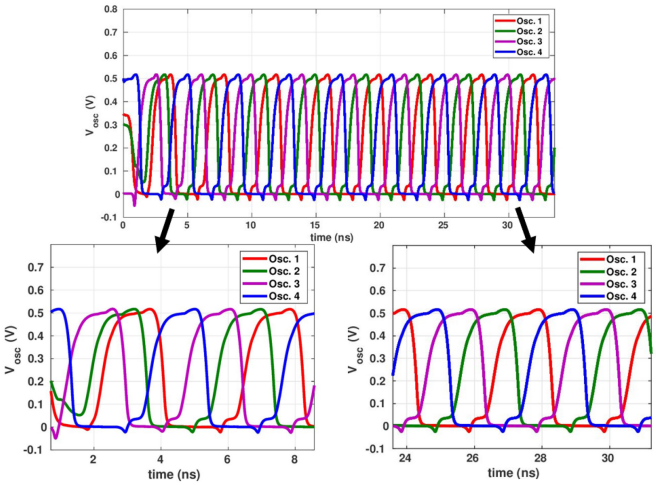

FIGURE 5. Output of high-order, injection-locked oscillatory neural network with four cells, where quadrature output phases correspond to a ground-state solution.

B. SIMULATION OF THE FOUR-COLORING THEOREM

The oscillator's ISF is simulated in SpectreRF using periodic transfer function (PXF) analysis. PXF simulation takes into account the folding of harmonics of the input current to the output oscillation voltage, at the frequency of interest [22]. The simulated ISF in Fig. 4 shows that $|\tilde{\Gamma}_1|$ is dominant. We intentionally design the ring oscillator to have asymmetric rise and fall times [23] in order to enhance $|\tilde{\Gamma}_4|$ and, therefore, the lock range for a given pump signal. A greater $|\tilde{\Gamma}_4|$ enables a weaker pump injection current to be used for each oscillator while still maintaining lock, reducing the total power consumption. In fact, from (20), the optimized ISF results in a wider lock range that enables robustness against free-running frequency variations among individual oscillators.

A transient noise simulation is run using SpectreRF and the high-order, injection-locked oscillatory neural network's outputs at V_4 node are shown in Fig. 5. In transient noise simulation, random noise sources are added to each device, at each time step. As a result, noise is superimposed onto the transient output waveforms, for a physically realistic simulation. For simplicity, the outputs at V_4 node are shown.

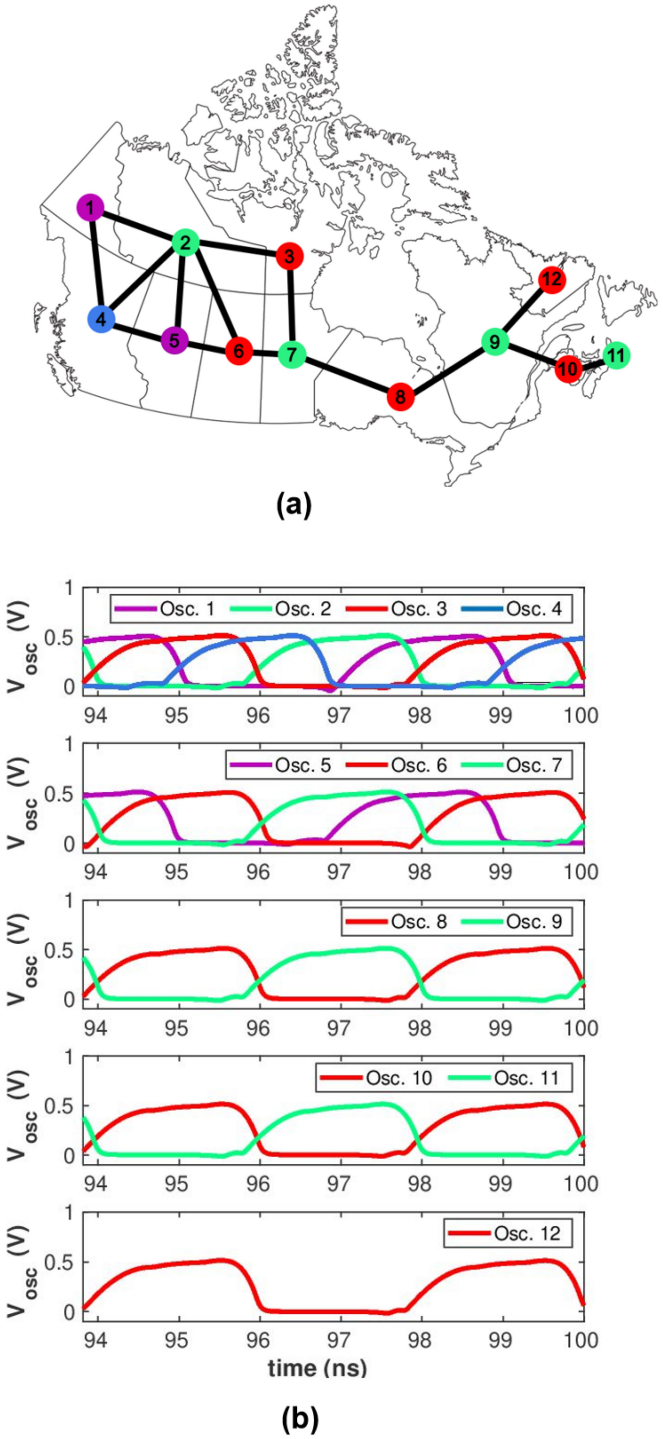

FIGURE 6. Coloring the map of Canada. (a) Output of high-order, injection-locked oscillatory neural network for a map of Canada's provinces and territories. (b) The output phases correspond to a ground-state solution and valid map coloring.

The oscillation frequency is 0.25 GHz, confirming that the oscillators are locked to a subharmonic of the 1 GHz pump signal. Initially, the oscillators have random phases, due to random initial conditions. A valid steady-state solution with

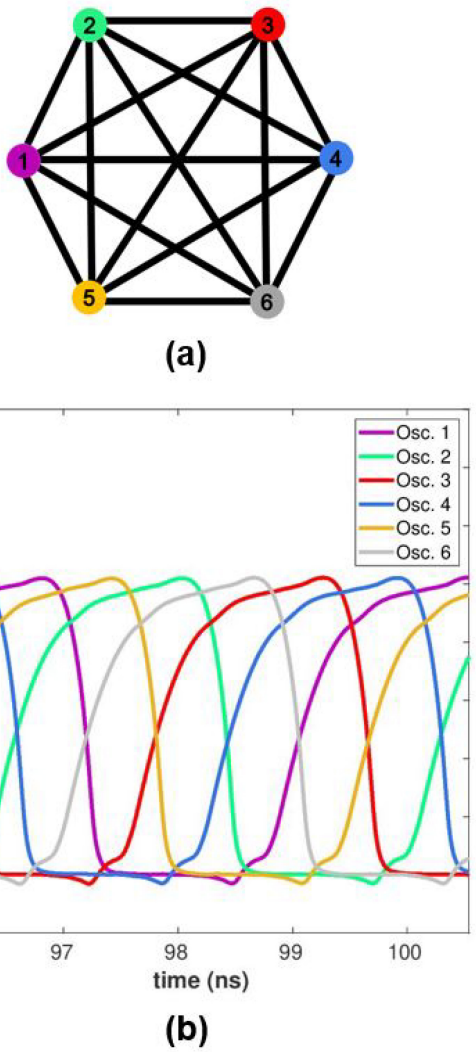

FIGURE 7. Coloring a non-planar graph. (a) Output of high-order, injection-locked oscillatory neural network for a six-colorable map. (b) The six output phases correspond to a ground-state solution and valid graph coloring.

the four different quadrature phases is reached within 30 ns. Assigning a color to each unique phase results in a coloring of the map, corresponding to the coloring in Fig. 1.

C. COLORING THE REGIONS OF A GEOGRAPHIC MAP

We now use a larger oscillatory CNN to color the map of Canada's contiguous provinces and territories, shown in Fig. 6. The equivalent graph has 12 vertices and 15 edges, which are mapped to 12 oscillators and 15 local bidirectional couplings (30 coupling connections), shown in Fig. 6. We use similar circuit blocks and coupling connections as the previous example. Again, we observe the map is four-colorable and the oscillators converge to quadrature phases. Assigning a color to each quadrature phase results in a valid coloring of the map of Canada.

D. COLORING THE VERTICES OF A NON-PLANAR GRAPH

We now extend our oscillatory CNN to color a non-planar graph, shown in Fig. 7. In this non-planar graph, the edges now cross at points other than the graph vertices. Since the graph is non-planar, the Four Color Theorem no longer applies, and six colors are required to color this graph. The equivalent graph has 6 vertices and 15 edges, which are mapped to 6 oscillators and 15 local bidirectional couplings (30 coupling connections), shown in Fig. 7. We use similar circuit blocks and coupling connections as the previous example. To realize six coloring with the oscillatory CNN, we now utilize divide-by-6 injection locking. Thus, the pump frequency is now 1.5 GHz, while the oscillation frequency is 250 MHz. We observe the map is six-colorable and the oscillators converge to six unique phases separated by 60°. Assigning a color to each unique phase results in a valid coloring of the non-planar graph.

V. CONCLUSION

We have proposed polychronous oscillatory cellular neural networks that use high-order injection-locked oscillators to solve graph coloring problems. We demonstrated how to apply the theory of the Potts model to the four-coloring problem and map it to a network of locally connected oscillators under divide-by-4 injection locking. We have used impulse sensitivity function (ISF) theory to model and optimize the injection locking of the oscillatory cellular neural network. We present CMOS circuit design examples and design guidelines. Spectre simulations confirm the CMOS oscillatory cellular neural network can color a geographic map, and therefore solve the four-coloring problem. The developed theory is general and is applicable to polychronous oscillatory cellular neural networks built using other devices whose ISF can be modeled, simulated, or measured. This architecture can be extended to solve other optimization problems.

ACKNOWLEDGMENT

The authors would like to thank Profs. Subhasish Mitra and Kwabena Boahen of Stanford University for valuable technical discussions. The authors wish to thank the anonymous reviewers for their constructive feedback on this manuscript.

REFERENCES

[1] S. Choudhary et al., "Silicon neurons that compute," in *Proc. Int. Conf. Artif. Neural Netw.*, 2012, pp. 121–128.
[2] C. Mead, *Analog VLSI and Neural Systems*. Boston, MA, USA: Addison-Wesley, 1989.
[3] M. Rastogi, V. Garg, and J. G. Harris, "Low power integrate and fire circuit for data conversion," in *Proc. IEEE Int. Symp. Circuits Syst.*, 2009, pp. 2669–2672.
[4] A. Neckar et al., "Braindrop: A mixed-signal neuromorphic architecture with a dynamical systems-based programming model," *Proc. IEEE*, vol. 107, no. 1, pp. 144–164, Jan. 2019.
[5] L. Chua and L. Yang, "Cellular neural networks: Theory," *IEEE Trans. Circuits Syst.*, vol. 35, no. 10, pp. 1257–1272, Oct. 1988.
[6] G. Manganaro, "Another look at cellular neural networks," in *Proc. Int. Workshop Cellular Nanoscale Netw. Appl. (CNNA)*, 2021, pp. 1–4.
[7] S. Duan, X. Hu, Z. Dong, L. Wang, and P. Mazumder, "Memristor-based cellular nonlinear/neural network: Design, analysis, and applications," *IEEE Trans. Neural Netw. Learn. Syst.*, vol. 26, no. 6, pp. 1202–1213, Jun. 2015.
[8] A. Ascoli, R. Tetzlaff, S.-M. Kang, and L. O. Chua, "Theoretical foundations of memristor cellular nonlinear networks: A DRM2-based method to design memcomputers with dynamic memristors," *IEEE Trans. Circuits Syst. I, Reg. Papers*, vol. 67, no. 8, pp. 2753–2766, Aug. 2020.
[9] A. Ascoli, M. Weiher, M. Herzig, S. Slesazeck, T. Mikolajick, and R. Tetzlaff, "Graph Coloring via locally-active memristor oscillatory networks," *J. Low Power Electron. Appl.*, vol. 12, no. 2, p. 22, 2022.
[10] Y. Kim, S. Shin, and K.-S. Min, "Shared memristance restoring circuit for memristor-based cellular neural networks," in *Proc. Int. Workshop Cellular Nanoscale Netw. Appl. (CNNA)*, 2014, pp. 1–2.
[11] S. Ziabakhsh, G. Gagnon, and G. W. Roberts, "The peak-SNR performances of voltage-mode versus time-mode circuits," *IEEE Trans. Circuits Syst. II, Exp. Briefs*, vol. 65, no. 12, pp. 1869–1873, Dec. 2018.
[12] E. M. Izhikevich and F. C. Hoppensteadt, "Polychronous wavefront computations," *Int. J. Bifurcat. Chaos*, vol. 19, no. 5, pp. 1733–1739, 2009.
[13] G. Buzsáki and A. Draguhn, "Neuronal oscillations in cortical networks," *Science*, vol. 304, no. 5679, pp. 1926–1929, 2004.
[14] R. M. R. Lewis, *A Guide to Graph Colouring: Algorithms and Applications*, 2nd ed. Cham, Switzerland: Springer, 2016.
[15] K. Appel and W. Haken, "Every planar map is four colorable. Part I: Discharging," *Illinois J. Math.*, vol. 21, no. 3, pp. 429–490, 1977.
[16] A. Crnkić, J. Povh, V. Jaćimović, and Z. Levnajić, "Collective dynamics of phase-repulsive oscillators solves graph coloring problem," *Chaos Interdiscipl. J. Nonlinear Sci.*, vol. 30, no. 3, Mar. 2020, Art. no. 33128.
[17] A. Parihar, N. Shukla, M. Jerry, S. Datta, and A. Raychowdhury, "Vertex coloring of graphs via phase dynamics of coupled oscillatory networks," *Sci. Rep.*, vol. 7, no. 1, p. 911, Apr. 2017.
[18] F. Y. Wu, "The Potts model," *Rev. Mod. Phys.*, vol. 54, pp. 235–268, Jan. 1982.
[19] A. Hajimiri and T. H. Lee, "A general theory of phase noise in electrical oscillators," *IEEE J. Solid-State Circuits*, vol. 33, no. 2, pp. 179–194, Feb. 1998.
[20] B. Hong and A. Hajimiri, "A general theory of injection locking and pulling in electrical oscillators—Part I: Time-synchronous modeling and injection waveform design," *IEEE J. Solid-State Circuits*, vol. 54, no. 8, pp. 2109–2121, Aug. 2019.
[21] R. L. Smith and T. H. Lee, "Modeling of injection locking in neurons for neuromorphic and biomedical systems," in *Proc. IEEE Int. Symp. Circuits Syst. (ISCAS)*, 2021, pp. 1–5.
[22] R. L. Smith and T. H. Lee, "Hybrid frequency domain simulation method to speed-up analysis of injection locked oscillators," in *Proc. IEEE Int. Midwest Symp. Circuits Syst. (MWSCAS)*, 2021, pp. 722–726.
[23] B. Hong and A. Hajimiri, "A general theory of injection locking and pulling in electrical oscillators—Part II: Amplitude modulation in *LC* oscillators, transient behavior, and frequency division," *IEEE J. Solid-State Circuits*, vol. 54, no. 8, pp. 2122–2139, Aug. 2019.
[24] H. Sakaguchi, S. Shinomoto, and Y. Kuramoto, "Local and grobal self-entrainments in oscillator lattices," *Progr. Theor. Phys.*, vol. 77, no. 5, pp. 1005–1010, May 1987.
[25] J. L. van Hemmen and W. F. Wreszinski, "Lyapunov function for the Kuramoto model of nonlinearly coupled oscillators," *J. Stat. Phys.*, vol. 72, no. 1, pp. 145–166, Jul. 1993.
[26] T. Wang and J. Roychowdhury, "OIM: Oscillator-based Ising machines for solving combinatorial optimisation problems," in *Proc. Int. Conf. Unconventional Comput. Nat. Comput. (UCNC)*, 2019, pp. 232–256.

RICHELLE L. SMITH (Graduate Student Member, IEEE) received the B.S. and M.S. degrees in electrical engineering-electrophysics from the University of Southern California, Los Angeles, CA, USA, in 2017, and the M.S. degree in electrical engineering from Stanford University, Stanford, CA, USA, in 2019, where she is currently pursuing the Ph.D. degree in electrical engineering.

She has held internship positions with Linear Technology, Milpitas, CA, USA; Rambus Labs, Sunnyvale, CA, USA; Stanford Brains in Silicon Laboratory, Stanford University; TDK-InvenSense, San Jose, CA, USA; and Silicon Laboratories, Austin, TX, USA. She holds four U.S. patents. Her research interests include energy-efficient systems, analog and RF integrated circuit design, wireline transceivers, and brain-inspired computing.

Ms. Smith was a recipient of the 2013 USC Trustee Full Tuition Scholarship, the 2013 Rambus Innovator of the Future Scholarship, the 2015 Tau Beta Pi Forge No. 42 Scholarship, the 2016 Barry Goldwater Scholarship, the 2016 Astronaut Scholarship, the 2017 NSF Graduate Research Fellowship, the 2017 Sang Samuel Wang Stanford Graduate Fellowship, the 2019 Analog Devices Outstanding Student Designer Award, the 2021 Cadence Women in Technology Scholarship, the 2022 ARCS Foundation Northern California Fellowship (William K. Bowes, Jr. Foundation Scholar), and the 2022–2023 IEEE SSCS Predoctoral Achievement Award.

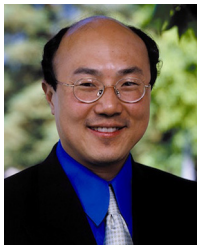

THOMAS H. LEE (Fellow, IEEE) received the S.B., S.M., and Sc.D. degrees in electrical engineering from the Massachusetts Institute of Technology, Cambridge, MA, USA, in 1983, 1985, and 1990, respectively.

He joined Analog Devices in 1990, where he was primarily engaged in the design of high-speed clock recovery devices. In 1992, he joined Rambus Inc., Mountain View, CA, USA, where he developed high-speed analog circuitry for 500 megabyte/s CMOS DRAMs. Since 1994, he has been a Professor of Electrical Engineering with Stanford University, Stanford, CA, USA, where his research focus has been on gigahertz-speed wireline and wireless integrated circuits built in conventional silicon technologies, particularly CMOS. He holds 65 U.S. patents and authored *The Design of CMOS Radio-Frequency Integrated Circuits* (currently, in its second edition) and *Planar Microwave Engineering* with Cambridge University Press. He is a coauthor of four additional books on RF circuit design, a Co-Founder of Matrix Semiconductor (acquired by Sandisk) and Ayla Networks, and the Founder of ZeroG Wireless (acquired by Microchip). He has also contributed to the development of PLLs in the StrongARM, Alpha, and AMD K6/K7/K8 microprocessors.

Dr. Lee has twice received the "Best Paper" Award at the International Solid-State Circuits Conference, coauthored a "Best Student Paper" at ISSCC, was awarded the Best Paper Prize at CICC, and is a Packard Foundation Fellowship recipient. In 2012, he was awarded the U.S. Secretary of Defense Medal for Exceptional Civilian Service, as well as an Honoris Causa Doctorate from the University of Waterloo. He served on Xilinx's Board of Directors from 2016 to its acquisition by AMD, was the 2011 Ho-Am Prize Laureate, and was awarded the IEEE Gustav Kirchhoff Award in 2021. He served for a decade as an IEEE Distinguished Lecturer of the Solid-State Circuits Society, and has been a DL of the IEEE Microwave Society as well. He is the past Director of DARPA's Microsystems Technology Office.